Weak crystallization theory of metallic alloys

Ivar Martin,[1] Sarang Gopalakrishnan,[2,3] and Eugene A. Demler[2]
[1]*Materials Science Division, Argonne National Laboratory, Argonne, Illinois 60439, USA*
[2]*Department of Physics, Harvard University, Cambridge, Massachusetts 02138, USA*
[3]*Department of Physics, California Institute of Technology, Pasadena, California 91125, USA*
(Received 25 June 2015; revised manuscript received 1 June 2016; published 20 June 2016)

Crystallization is one of the most familiar, but hardest to analyze, phase transitions. The principal reason is that crystallization typically occurs via a strongly first-order phase transition, and thus rigorous treatment would require comparing energies of an infinite number of possible crystalline states with the energy of liquid. A great simplification occurs when crystallization transition happens to be weakly first order. In this case, *weak crystallization theory*, based on unbiased Ginzburg-Landau expansion, can be applied. Even beyond its strict range of validity, it has been a useful qualitative tool for understanding crystallization. In its standard form, however, weak crystallization theory cannot explain the existence of a majority of observed crystalline and quasicrystalline states. Here we extend the weak crystallization theory to the case of metallic alloys. We identify a singular effect of itinerant electrons on the form of weak crystallization free energy. It is geometric in nature, generating strong dependence of free energy on the angles between ordering wave vectors of ionic density. That leads to stabilization of fcc, rhombohedral, and icosahedral quasicrystalline (iQC) phases, which are absent in the generic theory with only local interactions. As an application, we find the condition for stability of iQC that is consistent with the Hume-Rothery rules known empirically for the majority of stable iQC; namely, the length of the primary Bragg-peak wave vector is approximately equal to the diameter of the Fermi sphere.

DOI: 10.1103/PhysRevB.93.235140

I. INTRODUCTION

Crystals are best characterized in reciprocal space, where the onset of long-range order is signaled by the appearance of resolution-limited Bragg peaks. The intensity of the Bragg peaks reflects the density distribution in a material—for smooth density modulations, as in the case of liquid crystals, only a few harmonics of principal peaks located on a momentum shell of radius q_0 are needed to fully describe the state. The intensity of the principal harmonics plays the role of the order parameter in this case; when it is small near the transition (relative to the average density), the application of the Ginzburg-Landau theory is justified. In atomic crystals, typically, density is highly concentrated near the equilibrium positions of atoms, and the number of relevant Bragg-peak harmonics scales in proportion to the ratio of the unit cell size to the atomic size (smeared by thermal and quantum fluctuations). In a typical crystal, the thermal fluctuations of atoms are 15–30% of the lattice spacing at the melting transition [1]; therefore, to accurately describe the transition, multiple harmonics of q_0 are required [2,3]. The appearance of strong modulation immediately at the phase transition, with multiple Bragg peaks forming a reciprocal lattice, is the signature of a strongly first-order transition.

Weak crystallization theory [4,5] applies Ginzburg-Landau machinery to the crystallization problem by assuming that only principal Bragg peaks located on momentum shell q_0 significantly contribute to energy. Even though it most directly applies only to liquid crystals and polymers [6], it has been successful in predicting the ubiquity of body-centered-cubic (bcc) crystals near crystallization temperature [7]. In this way, it has been a useful symmetry-based tool to study the crystallization transition, even beyond its immediate range of validity. In the standard—spatially local—form, however, weak crystallization theory is incapable of obtaining many of the experimentally observed crystalline states, such as simple cubic, rhombohedral, or face centered cubic (fcc), while its heuristic modifications that allow one to obtain some of these states have not been microscopically justified.

The crystal structure depends on a variety of details, such as ionic charge and electronic orbital structure, etc., which lead to an immense variety of natural and synthetic crystals. Remarkably, in the case of metallic alloys, simple empirical rules exist that connect crystal structure and the composition of alloys. These rules were identified by Hume-Rothery [8] who has found that metallic alloys are particularly stable when, in addition to the requirement that atoms be of similar size and electronegativity, the value of the average valence per atom ("e/a" ratio) has to be close to certain "magic" values, which depend on the crystal structure. Subsequently, the optimal e/a ratios have been argued to be associated with a particular geometrical matching condition, when the itinerant (nearly free) electron Fermi surface "just crosses" the boundary of the first Brillouin zone [9]. Regardless of interpretation, this observation highlights the important role that itinerant electrons play in determining the crystal structure. This is indeed not surprising given that itinerant electrons can effectively mediate long-range and multi-ionic interactions.

A special case of a metallic crystalline solid is a *quasicrystal*. In quasicrystals, atoms lack simple spatial periodicity, yet, in the reciprocal space, resolution-limited Bragg peaks appear in a self-similar arrangement inconsistent with crystallographically allowed point-group symmetries [10–14]. Significantly, the majority of stable quasicrystals are Hume-Rothery alloys [15,16], i.e., they are stable for narrow ranges of e/a. Despite nominally large conduction electron concentration, their electrical and thermal conductivities are exceptionally low [17,18], consistent with strong scattering around the Fermi surface. These observations led to attempts to construct a theory of quasicrystals accounting for the

 ©2016 American Physical Society

Hume-Rothery rules by perturbatively including electron scattering on quasiperiodic ionic potential [19]. Just as in the case of regular crystals, such approach is problematic since comparison of different ordered states requires the knowledge of the magnitude of the modulated ionic potential (see Appendix A). Weak crystallization theory, with some phenomenological modifications, has also been invoked to address the problem of stability of quasicrystals [20–24]. However, without including electrons explicitly, it cannot account for the appearance of the Hume-Rothery rules in quasicrystals.

Here we extend the weak crystallization theory to metallic systems. This method is unbiased in the sense that no assumptions regarding the ionic potentials are needed, and the energies of different crystalline and quasicrystalline states can be directly compared. The weakness of the method is that it applies, strictly speaking, only to the weakly first-order transitions, and hence in many practical situations its results can only be taken qualitatively. Nevertheless, the singular features that we identify in the fourth-order Ginzburg-Landau theory due to electrons are geometrical in nature (being higher-order analogs of the Peierls instability), and thus should remain important even beyond the assumptions of the weak crystallization theory.

Within our approach, the Hume-Rothery rules emerge from the interplay of two length scales—the preferred interionic distance, $1/q_0$, and the Fermi wavelength of itinerant electrons, $1/k_F$. We find that interionic interactions generated by electrons qualitatively modify the generic weak crystallization theory, stabilizing fcc, rhombohedral, and, notably, icosahedral quasicrystal (iQC) states. Even though we find that numerically these phases are stabilized near $q_0 \approx 2k_F$, the physical and geometric meaning of this condition in our case is completely different from the Fermi surface "nesting" of Jones [9].

It should be mentioned that density functional theory appropriate for the case of strongly first-order crystallization [2] has also been applied to the problem of energetic stability of quasicrystals [25]. The great appeal of such theories is that by taking only the properties of the liquid as an input (e.g., the structure factor), they can predict the properties of the solids in the coexistence phase. The weakness, however, is that being inherently phenomenological, they cannot explicitly account for the role of electrons and, hence, the occurrence of the Hume-Rothery rules. The systematic expansion in terms of electron-ion interactions that we perform here is implicit within these liquid parameters.

II. WEAK CRYSTALLIZATION THEORY AND ITS EXTENSION TO METALS

In what follows, we shall keep only momenta of length q_0; i.e., we shall make the ansatz $\rho(\mathbf{x}) = \rho_0 + \sum_{|\mathbf{k}|=\mathbf{q_0}} \mathrm{Re}[\rho_{\mathbf{k}} e^{i\mathbf{k}\cdot\mathbf{x}}]$ for ionic density. As discussed above, this ansatz, which is central to "weak crystallization" theory [5], is strictly valid only where the crystallization transition is weakly first order and its latent heat is small. Outside this regime, our results will not be quantitatively accurate; nevertheless, we expect them to provide guidance as to what kinds of crystal structures are favored.

We proceed by writing a general Ginzburg-Landau (GL) free-energy functional, $\mathcal{F} = F_0 + H_0 + V$, where

$$F_0 = \sum_{\mathbf{q}} r(q)|\rho_{\mathbf{q}}|^2 + \frac{\lambda_3}{3!}\sum_{\mathbf{q}_i} \rho_{q_1}\rho_{q_2}\rho_{q_3}\delta\Big(\sum q_i\Big) + \frac{\lambda_4}{4!}\sum_{\mathbf{q}_i} \rho_{q_1}\rho_{q_2}\rho_{q_3}\rho_{q_4}\delta\Big(\sum q_i\Big), \quad (1)$$

$$H_0 = \sum_{\mathbf{k}} [E(k) - \mu] c^\dagger_{\mathbf{k}} c_{\mathbf{k}}, \quad (2)$$

$$V = \sum_{\mathbf{kq}} v(q)\rho_q c^\dagger_k c_{k-q}. \quad (3)$$

Here, F_0 describes the physics of ions and *core* electrons in the absence of itinerant electrons. The minimal ("local") assumption that is commonly made is that interactions λ_3 and λ_4 are mere constants. However, as interatomic interactions set a preferred length scale for crystallization even in the absence of conduction electrons, this length scale is introduced into the second-order term, via the weak crystallization form $r(q) = r_0 + \chi(|q| - q_0)^2$. As already stated, we will restrict our attention to density modes that are precisely at $q = q_0$ [26]. The second term H_0 describes the itinerant electrons: for simplicity, we shall treat these as noninteracting. The third term V describes the interaction between itinerant electrons and atoms. As we are only concerned with density modulations satisfying $q = q_0$, and the interaction is assumed to be spherically symmetric, we can parametrize the interaction strength entirely by its Fourier component at momentum transfer q_0, viz., $v \equiv v(q_0)$. Thus we need not make any assumptions about screening of the Coulomb interaction. The kinematic constraints $\sum_{\mathbf{q}_i}$, in combination with the $q = q_0$ restriction, strongly limit the number of allowed terms. Namely, the cubic term is only nonzero for triplets of $\mathbf{q}_i$ forming equilateral triangles, and thus favors hexagonal and bcc crystal structures [7]. The quartic term obtains generically from combining $\pm\mathbf{q}_i$ with $\pm\mathbf{q}_j$. It can also appear in the situation when four $\mathbf{q}_i$ form a noncoplanar quadrilateral [e.g., the geometry in Fig. 1(a)].

III. ELECTRONIC CONTRIBUTION TO WEAK CRYSTALLIZATION ENERGY FUNCTIONAL

We now integrate out the conduction electrons to arrive at a description that is purely in terms of the ionic densities. The procedure is analogous to the derivation of the Ginzburg-Landau functional for superconductivity or charge density wave states [27]. The difference is that the ionic density order parameter, *a priori*, can have an arbitrary number of components, and the energy functional should be able to predict not only the magnitude of the order parameter, but also the number and orientation of its components. The latter determine the type of crystalline state.

As the free-energy functional $\mathcal{F} = F_0 + H_0 + V$ is quadratic in fermion operators, we can integrate out the fermions; this allows us to write the partition function purely in terms of ionic densities, as $\mathcal{Z} = \exp[-\beta(F_0 - \Delta F)]$ where F_0 is defined in Eq. (1) and ΔF is given by the following perturbation series, which we have resummed using the linked

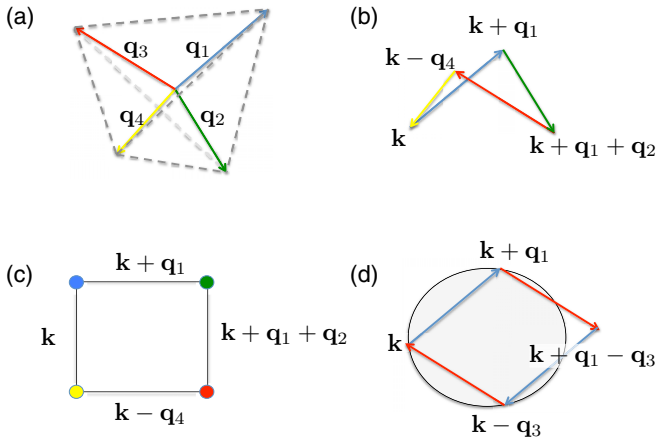

FIG. 1. (a) First shell of reciprocal lattice vectors for the case of fcc real-space (bcc reciprocal) lattice vectors. Four vectors point from the center of a tetrahedron to its vertices. (b) Example of a scattering path between electronic momentum states induced by the ionic densities modulated at wave vectors in (a). This process makes contribution to $w(\{\mathbf{q}_i\})$ in Eq. (4). (c) Feynman "box" diagram for the fourth-order contribution to the GL free energy. Lines correspond to electronic Green functions; vertices correspond to ionic densities with a given wave vector. (d) An example of coplanar contribution to free energy that only contains two pairs of $\pm\mathbf{q}_i$ [a contribution to $u(q_0,\alpha_{ij})$]. As shown, it corresponds to the "resonance" conditions satisfied: three or more electronic momenta are on a great circle of the Fermi surface.

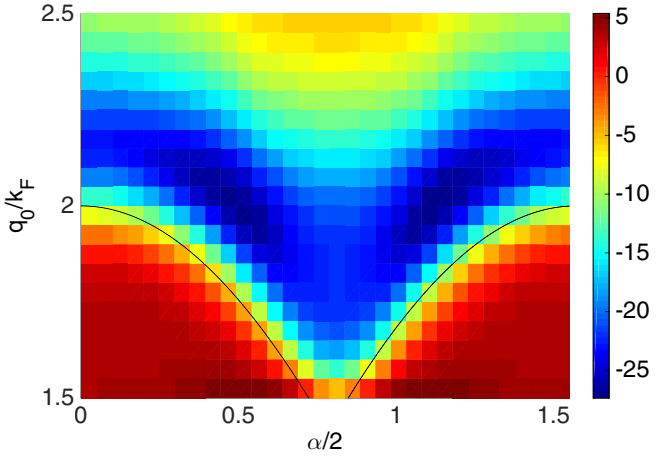

FIG. 2. Electronic contribution $u(\alpha)$ to the fourth-order term in the Ginzburg-Landau energy functional given by Eq. (4). Temperature is $T = 0.1E_F$. Black lines mark the location of zero-temperature singularity, $Q/k_F = 2\cos\frac{\alpha}{2}$.

cluster theorem:

$$\Delta F = -\frac{1}{\beta}\sum_n \frac{(-1)^n}{n}\int d\tau_1 \ldots d\tau_n \langle \mathcal{T}_\tau V(\tau_1)\ldots V(\tau_n)\rangle_{conn}.$$

Explicit expressions are given in Appendix B. We now expand ΔF to quartic order in the bosonic densities; this yields, for the free-energy functional $F \equiv F_0 + \Delta F$,

$$F = \sum_{\mathbf{q_i}} \tilde{r}(q)|\rho_{\mathbf{q}}|^2 + \tilde{\lambda}_3(q_0)\sum_{\triangle}\rho_{\mathbf{q}_1}\rho_{\mathbf{q}_2}\rho_{\mathbf{q}_3}\delta\Big(\sum \mathbf{q}_i\Big) + \frac{1}{2}\sum_{\mathbf{q}_i\neq\mathbf{q}_j}[\lambda_4 + u(\alpha_{ij})]|\rho_{\mathbf{q}_i}|^2|\rho_{\mathbf{q}_j}|^2 + \frac{1}{4}\sum_{\mathbf{q}_i}[\lambda_4 + u(0)]|\rho_{\mathbf{q}_i}|^4 + \sum_{\square}[\lambda_4 + w(\{\mathbf{q}_i\})]\rho_{\mathbf{q}_1}\rho_{\mathbf{q}_2}\rho_{\mathbf{q}_3}\rho_{\mathbf{q}_4}. \quad (4)$$

The symbols $\sum_\triangle$ and $\sum_\square$ indicate summation over unique triangles and nonplanar quadrilaterals of $\mathbf{q}_i$; α_{ij} is the angle between vectors $\mathbf{q}_i$ and $\mathbf{q}_j$.

Numerical results

Figure 2 shows $u(\alpha)$ for various values of q_0 at $T = 0.1E_F$. Already at this not very low temperature, certain features become apparent. For $q_0/k_F \sim \sqrt{2}$, a minimum in $u(\alpha)$ develops around $\alpha = \pi/2$, which then splits into two minima for larger values of q_0. In the limit of zero temperature, a singularity develops along the line $q_0/k_F = 2\cos\frac{\alpha}{2}$. Geometrically, this condition corresponds to the configuration when three momenta connected by scattering off the ionic order parameter, $\mathbf{k}$, $\mathbf{k}+\mathbf{q}_1$, and $\mathbf{k}+\mathbf{q}_2$, can all simultaneously be on a great circle of the Fermi surface [Fig. 1(d)]. Near this line, the vertex is repulsively divergent for smaller q_0 and attractively divergent for larger q_0 as $T \to 0$. This singular behavior is a four particle/hole analog of the particle-hole divergence in one dimension (1D) that drives Peierls instability. Naturally, such a strong angular dependence of $u(\alpha)$ at temperatures much lower than E_F can influence the energetic balance between different crystalline phases. It should be noted that the angular dependence is a result of a sharply defined Fermi surface; at temperatures comparable to or higher than the Fermi energy, it becomes smeared out.

The noncoplanar terms $w(\{\mathbf{q}_i\})$ are less generic than $u(\alpha)$ since they require four distinct wave vectors to add up to zero. A case where these terms are important is the fcc crystal, whose first Bragg shell (the set of shortest symmetry-related reciprocal lattice vectors) is comprised of eight vertices of a cube; hence there are two nontrivial quadruplets of wave vectors that correspond to the vertices of two tetrahedra (see Fig. 1). The significance of noncoplanar terms is that they can always be made to lower energy by appropriate choice of the relative signs of constituent $\rho_{\mathbf{q}_i}$. For the momentum-independent interactions, this does not change the fact that the stripe state has the lowest energy within weak crystallization theory. However, inclusion of the electron-induced interaction can change the situation dramatically. In Fig. 3, we plot $w(\{\mathbf{q}_i\})$ as a function of q_0 for fcc. We find that it has features similar to $u(\alpha)$; namely, when $q_0/k_F = 2\cos\frac{\alpha_t}{2}$, with $\alpha_t = \arccos(1/3)$ the tetrahedral angle, w diverges as $T \to 0$. This enhanced interaction is the cause of a large region of stability of fcc phase that we find.

IV. PHASE DIAGRAM

To construct the phase diagram, we first consider the set of variational states that contain N pairs of $\pm\mathbf{q}_i$, where all $\mathbf{q}_i$'s are symmetry related and hence have exactly the same set of neighbors. Then, all of the Fourier amplitudes are identical,

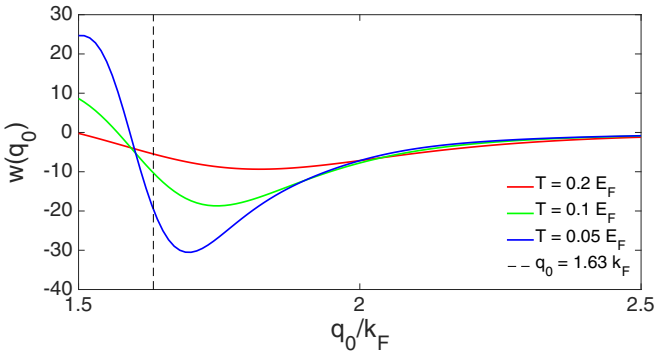

FIG. 3. Temperature and q_0 dependence of noncoplanar electronic contribution $w(q_0)$ to the fourth-order term in Ginzburg-Landau energy for fcc crystal. The black vertical line marks the location of zero-temperature singularity, $q_0/k_F = 2\cos\frac{\alpha}{2}$, where $\alpha = \arccos(1/3)$.

$|\rho_{\mathbf{q}_i}| = \rho$, and the free energy is

$$F = Nr_0|\rho|^2 + \frac{N}{2}\left[\sum_{j\neq 0}\tilde{u}(\alpha_{0j}) + \frac{\tilde{u}_0}{2} - \frac{2M_\square}{N}|\tilde{w}(\{\mathbf{q}_i\})|\right]|\rho|^4,$$

where we redefined $\tilde{u} = u + \lambda_4$ and $\tilde{w} = w + \lambda_4$ for compactness. We assumed that all $M_\square$ quadruplets have the same $w(\{\mathbf{q}_i\})$ (the case for fcc) and that vectors q_i do not form equilateral triangles, and hence the cubic invariant that could stabilize bcc (fcc reciprocal) crystal does not contribute (the latter assumption should become valid for sufficiently large negative r_0). Now it only remains to minimize the energy to obtain

$$|\rho|^2 = -\frac{r_0}{\sum_{j\neq 0}\tilde{u}(\alpha_{0j}) + \frac{\tilde{u}_0}{2} - \frac{2M_\square}{N}|\tilde{w}(\{\mathbf{q}_i\})|}$$

and

$$F = -\frac{r_0^2}{\frac{2}{N}\sum_{j\neq 0}\tilde{u}(\alpha_{0j}) + \frac{\tilde{u}_0}{N} - \frac{4M_\square}{N^2}|\tilde{w}(\{\mathbf{q}_i\})|}. \quad (5)$$

It is important to note that the pure electronic vertex u is negative (attractive) in a wide range of q_0 and α, which taken by itself could cause an absolute instability. In this regime, one cannot truncate F at fourth order, but must include higher-order terms in the GL expansion to find stable equilibrium states. However, the structureless local interaction λ_4 restores stability while maintaining the strong angle dependence of the interactions.

The results of our analysis are presented in Fig. 4. We find only four stable phases: rhombohedral, striped, fcc, and iQC (i.e., icosahedral quasicrystal). The other symmetric variational states we explored are always higher in free energy than these (see lower panel of Fig. 4 for energy comparison and Appendix C for details of the variational states). The overall shape of the phase diagram can be understood as follows. When the structureless interaction λ_4 is absent or too weak, as noted above, the free energy can become unbounded from below at quartic order. On the other hand, when λ_4 is dominant, the electron-induced interaction can be ignored, and we recover the standard weak crystallization result that the equilibrium state is striped (or smectic). When we are

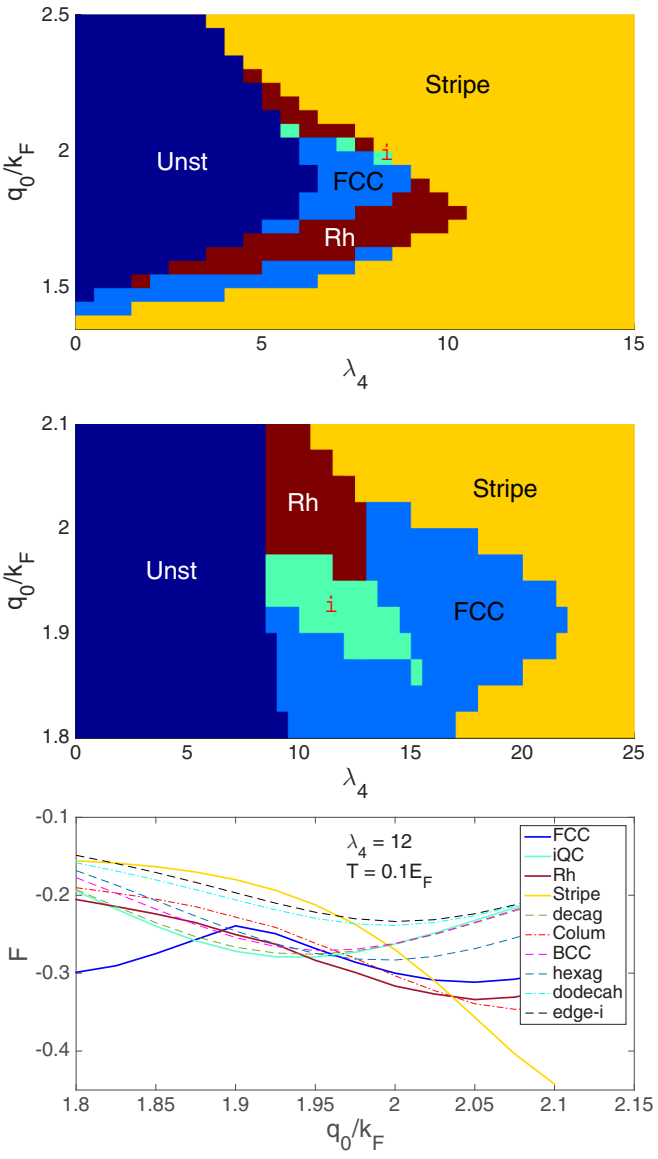

FIG. 4. Variational phase diagram for $T = 0.2E_F$ (top panel) and $T = 0.1E_F$ (middle panel) as a function of local repulsion strength λ_4 and the ionic ordering vector q_0. At small values of λ_4 (region marked Unst), the fourth-order terms in GL for one or more of the variational states becomes negative, signaling the need to consider higher-order stabilizing terms. The lower panel shows an energy comparison of different variational states for a fixed value of λ_4 at $T = 0.1E_F$.

far from the matching condition $q_0 \sim 2k_F$ or the temperature is relatively high, the interactions are not strongly angle dependent, and these are the two dominant possibilities. On the other hand, when the structureless and electronic contributions are of similar magnitude *and* the temperature is low, the angle dependence of the electron-mediated interaction stabilizes nontrivial crystalline phases.

The most significant qualitative feature of the phase diagram for intermediate values of λ_4 is the dominance of fcc and rhombohedral phases, with balance shifting in favor of fcc at lower temperatures. The reason for this trend is that fcc has two appealing features: (1) it has only one inter-$\mathbf{q}$ angle α_{ij} (up to $\pi - \alpha_{ij}$), and (2) it has lower energy due to the presence of

noncoplanar fourth-order terms. Rhombohedral crystal only has the former feature, and thus only becomes competitive when the angle $\alpha_{\min}$ that minimizes $u(\alpha)$ is sufficiently far from the tetrahedral angle. Surrounded by the fcc and rhombohedral phases is the iQC phase. The key advantage of the iQC phase is that it has a large number (six) of $\pm\mathbf{q}_i$ pairs, all separated by the same angle $\alpha_i = 2\sin^{-1}(\gamma^2+1)^{-1} \approx 63.43^\circ$ (γ is the Golden mean). Even though iQC cannot benefit from the noncoplanar energy terms, when the optimal angle $\alpha_{\min}$ is close to the α_i, iQC can beat both fcc and rhombohedral. Finally, for large λ_4, we recover the stripe phase predicted by the original featureless weak crystallization theory.

Except for the fcc phase with its noncoplanar terms in energy, the phase diagram can be understood as follows. For the states with only one nontrivial inter-$\mathbf{q}$ angle $\alpha_{\min}$, the denominator in Eq. (5) is $\tilde{u}(\alpha_{\min}) + [\tilde{u}(0) - 2\tilde{u}(\alpha_{\min})]/N$. Thus, if the second term is positive, it favors large N; if it is negative, then $N = 1$. Note that for $u(0) = 2u(\tilde{\alpha})$, states with all possible N's are energetically degenerate [can be seen in the triple crossing point in Fig. 4 (lower panel) at $q_0/k_F \approx 2.05$].

A. Distorted states

In construction of the phase diagram, we have only considered highly symmetric states. We now discuss possible deviations from these assumptions. First, we can ask whether the highly symmetric crystal states are stable with respect to "Bragg fractionalization," namely whether it may be beneficial to split Bragg peaks into multiple nearby ones. From the fact that $\tilde{u}(\alpha \to 0) = \tilde{u}_0$, which can be explicitly demonstrated for electron-mediated and local interaction, for $\tilde{u}_0 > 0$, lack of fractionalization follows trivially (see Appendix D). The next possibility is a distortion of peaks from symmetric positions. Clearly this is not a concern for the rhombohedral state, but could be for iQC and fcc. Here we specifically ask whether iQC will remain stable even if $\alpha_{\min}$ is not exactly α_i (see Appendix E). Due to its high symmetry, iQC cannot naturally distort, unlike, e.g., the rhombohedral state. To answer this question, we have expanded the interaction energy around the symmetric iQC state. We have found that if $u'(\alpha_i) < -(2/3)u''(\alpha_i)$, then iQC spontaneously distorts into a lower symmetry state, i.e., a distortion could occur if $\alpha_{\min} > \alpha_i$ ("compressed springs"). This criterion also shows that if $u(\alpha)$ is sufficiently smooth, as it is for temperatures not very much smaller than the Fermi energy, then undistorted iQC should in fact be quite stable. Indeed, expanding around $\tilde{\alpha}$, we find that the criterion for instability is $\tilde{\alpha}_{\min} - \alpha_i > 2/3$, i.e., the minimum is at least 40° away (above) from the icosahedral angle. This estimate is based on the assumption of smoothness of $u(\alpha)$, which is violated at temperatures sufficiently below the Fermi temperature. Thus, for quasicrystals that form under such conditions, there is a possibility of distorted iQC, as well as a structural transition from perfect to distorted iQC as a function of temperature.

B. Stochastic energy minimization

We have also explored possible ordered states in an alternative fashion by applying unconstrained stochastic minimization of the free-energy functional. To simplify simulations, we neglected the cubic and noncoplanar quartic terms and thus cannot fully capture fcc and bcc phases; however, the advantage of this method is that it provides an unbiased treatment for arbitrary multi-q states that are not required to possess any special symmetries. We start from random configuration of several hundred components $\rho_{\mathbf{q}_i}$ with $\mathbf{q}_i$ on a sphere of radius q_0. We then iteratively minimize energy by randomly selecting $\rho_{\mathbf{q}_i}$ and changing its value and position on q_0 sphere in the direction of decreasing energy. The minimization results are consistent with the variational phase diagram in Fig. 4 (modulo underestimating the stability of fcc). Due to the stochastic nature of the algorithm, however, it sometimes converges to other states. In particular, in the region of stability of iQC, the final state is rather commonly the decagonal state, which is approximately the iQC state with one pair $\pm q_i$ removed. This state is an example of a 2D quasicrystal—it is periodic along one axis and quasiperiodic in the plane perpendicular to it. Even though the energy of this state is very close to the iQC, we have not observed it ever to be lower in energy than the perfect iQC [consistent with Fig. 4 (lower panel)]. The energy difference is nevertheless sufficiently delicate, so one cannot rule out that for modified conditions, the decagonal state may appear as the lowest-energy state in the phase diagram.

V. DISCUSSION

The conjecture that stability of 3D quasicrystals is associated with "bond-orientational order" that favors specific inter-$\mathbf{q}_i$ angles within weak crystallization theory has been previously proposed by Mermin and Troian [23] and Jaric [22]. In Ref. [23], an auxiliary field was introduced to generate preferred inter-$\mathbf{q}_i$ angle; however, no physical justification was given as to the nature of this field. The key result of our work is that itinerant electrons play the role similar to the auxiliary field postulated in [23]. On the experimental side, it has been found that the optimal e/a ratio observed in quasicrystals corresponds to the approximate matching between the quasicrystalline *quasi*-Brillouin zone and the electronic Fermi surface; that is, the length of the dominant Bragg wave vector approximately equals the diameter of the Fermi surface, $2k_F$. This is indeed what we find (Fig. 4).

It is interesting to note that related physics takes place in Faraday ripple patterns that appear on a liquid surface upon vertical driving. In this system, the Lyapunov function assumes the role of the Ginzburg-Landau functional. Various crystalline and quasicrystalline patterns emerge as a direct consequence of the angular dependence of the fourth-order coefficient of the Lyapunov function [28,29].

VI. CONCLUSIONS

In conclusion, we have analyzed the effects of electron-ion interactions on crystallization transition within weak crystallization theory. We found that the angular-dependent multi-ion interactions induced by electrons can lead to stabilization of such empirically common but elusive (within the standard theory) states as rhombohedral, fcc, and icosahedral quasicrystals. The stability conditions give a physical interpretation of the

Hume-Rothery rules connecting primary ionic ordering wave vectors and the size of the electronic Fermi surface. Our results are obtained within the assumption that the cubic invariants are less relevant than the quartic ones, i.e., at temperatures sufficiently lower than the temperature of the mean-field transition ($r_0 = 0$). Near the transition, more careful analysis of fluctuations is required [30], which will be the subject of future work.

ACKNOWLEDGMENTS

Authors would like to thank P. Goldbart, Z. Nussinov, D. Levine, P. Steinhardt, J. Vinals, and A. Rosch for useful discussions. I.M. acknowledges support from Department of Energy, Office of Basic Energy Science, Materials Science and Engineering Division. S.G. and E.A.D. acknowledge support from Harvard-MIT CUA, NSF Grant No. DMR-1308435, and AFOSR Quantum Simulation MURI. S.G. acknowledges support from the Walter Burke Institute at Caltech. E.A.D. acknowledges support from the Humboldt Foundation.

APPENDIX A: OTHER APPROACHES TO CRYSTALLIZATION THEORY AND THEIR LIMITATIONS

The most common approach to determine the lowest-energy crystal structure is based on variants of microscopic density functional theory, which specifies atoms with their electronic shells and variationally optimizes their spatial arrangement [31]. Due to computational complexity, this approach can effectively treat only periodic arrangements of atoms. Near the melting transition, application of this method becomes difficult since atoms in a liquid lack spatial periodicity. In that regime, methods combining density functional theory with molecular dynamics are applied, but only with limited success [32–34].

Periodic *approximants* to quasicrystals have also been studied by density functional theory [35]; application of this method, however, requires a very large number of atoms to be explicitly considered and optimized for the approximants' energies to provide a good estimate for quasicrystals, even away from the melting transition.

Another, semimicroscopic approach is based on the Peierls instability-type arguments. There, one studies the features in the electronic susceptibility and attempts to use its anomalies as a predictor of stable phases. This approach is problematic in the case of 3D alloys, as can be easily seen. We would like to have an unbiased predictor of an ordered state; therefore, the only starting point possible is a free-electron Fermi sea coupled to featureless (constant) ionic density. In 1D, electronic susceptibility diverges at $2k_F$ at $T = 0$, which leads to a density instability at this wave vector; this is the origin of charge density waves in many quasi-1D materials. In contrast, in 3D, free-electron susceptibility is maximized at zero momentum, and at $2k_F$ only has infinite first derivative (the cause of Friedel oscillations of electron-mediated interaction [36–38]). However, this is insufficient to cause instability in ionic density—theory would predict that the instability should occur at zero wave vector, i.e., at uniform density. Moreover, the (quadratic) term in the GL theory that is proportional to the electronic susceptibility only includes a single density modulation, and thus cannot discern between orderings that contain multiple wave vectors.

A way to go beyond the quadratic energy approximation is to include the ionic modulation nonperturbatively in electron dispersion [9]. It has been argued this way that for a given crystal structure, the electronic energy is minimized when the Fermi surface "just crosses" the Brillouin-zone boundary. This naturally corresponds to crystal-specific optimal e/a ratios, and thus appears to be consistent with the empirical Hume-Rothery rules. Application of this approach to discriminate between energies of different crystalline and quasicrystalline states is, however, problematic, as it presupposes the knowledge of the amplitude of the periodic lattice (pseudo)potential, which is different for different crystals. Since the energies of various states are typically rather similar, the uncertainty in the potential makes such approach unreliable.

APPENDIX B: DETAILS OF ELECTRONIC CORRECTIONS TO FREE ENERGY

Integration of electronic degrees of freedom leads to the following corrections to the ionic free-energy functional:

$$\Delta F^{(2)} = -\frac{1}{2\beta}\int d\tau_1 d\tau_2 \left\langle \mathcal{T}_\tau \sum_{k_1,q_1,k_2,q_2} v_{q_1}\rho_{q_1} c^\dagger_{k_1+q_1} ck_1|_{\tau_1} v_{q_2}\rho_{q_2} c^\dagger_{k_2+q_2} ck_2|_{\tau_2} \right\rangle_{conn} \tag{B1}$$

$$= \frac{|v_q\rho_q|^2}{2\beta}\int d\tau_1 d\tau_2 G_p(\tau_2-\tau_1)G_{p-q}(\tau_1-\tau_2) = \frac{|v_q\rho_q|^2}{2\beta}\sum_{\omega_n,p} G_p(\omega_n)G_{p-q}(\omega_n), \tag{B2}$$

$$\Delta F^{(3)} = -\frac{v^3_{q_0}\rho_{q_1}\rho_{q_2}\rho_{q_3}\delta\left(\sum q_i\right)}{3\beta}\sum_{\omega_n,p} G_p(\omega_n)G_{p-q_1}(\omega_n)G_{p-q_1-q_2}(\omega_n), \tag{B3}$$

$$\Delta F^{(4)} = \frac{v^4_{q_0}\rho_{q_1}\rho_{q_2}\rho_{q_3}\rho_{q_4}\delta\left(\sum q_i\right)}{4\beta}\sum_{\omega_n,k} G_p(\omega_n)G_{p-q_1}(\omega_n)G_{p-q_1-q_2}(\omega_n)G_{p-q_1-q_2-q_3}(\omega_n). \tag{B4}$$

Here, $G_p(\omega_n) = (i\omega_n - \epsilon_p)^{-1}$.

As one can see, the new terms in the Ginzburg-Landau functional have the form similar to those already contained in F_0 [Eq. (1)]. The second-order term $\Delta F^{(2)}$ only serves to redefine q_0 and hence will be of no interest to us. The prefactor of the cubic term becomes a function of q_0. We find

by numerical integration that the electronic contribution to this term is nonsingular in the limit of zero temperature, and thus it does not introduce any qualitatively new features relative to those already in F_0.

The fourth-order correction $\Delta F^{(4)}$ can diverge if certain geometric conditions are satisfied (see Fig. 1 of the main text). Thus we concentrate here on this term only.

The first type of fourth-order term that we will consider is self-interaction. Self-interaction is generated by box diagrams with momentum transfers $(\mathbf{q}_1,\mathbf{q}_1,-\mathbf{q}_1,-\mathbf{q}_1)$ (type A) and $(\mathbf{q}_1,-\mathbf{q}_1,\mathbf{q}_1,-\mathbf{q}_1)$ (type B). The combinatorial multiplicities of these diagrams can be calculated as follows. At every vertex of the box diagram, we can place $\rho_{\pm\mathbf{q}_1}$. For A type, there the sign pattern has to be such that same signs are adjacent, while for B, they are interlaced. There are four ways to place two adjacent $++$ in four boxes: $(++--)$, $(-++-)$, $(--++)$, $(+--+)$. Hence, A type has multiplicity 4. For B type, there are only two distinct ways to arrange: $(+-+-)$, $(-+-+)$, and multiplicity is 2. Therefore, the self-interaction goes as

$$\sum_i (4A+2B)|\rho_{q_i}|^4.$$

There are two types of mutual interaction diagrams: those that contain only two pairs of $\pm\mathbf{q}_i$ ("coplanar" diagrams) and those that contain four distinct $\mathbf{q}_i$'s ("noncoplanar" diagrams). Coplanar diagrams depend only on one angle between $\mathbf{q}_1$ and $\mathbf{q}_2$ (for $\alpha=0$, we get self-interaction). There are three distinct contributions to $\Delta F^{(4)}$, which come from the following arrangements or momenta around the box diagram: $\Delta F_1^{(4)}$: $(\mathbf{q}_1,-\mathbf{q}_1,\mathbf{q}_2,-\mathbf{q}_2)$ (type V_1), $\Delta F_2^{(4)}$: $(\mathbf{q}_1,-\mathbf{q}_1,-\mathbf{q}_2,\mathbf{q}_2)$ (type V_2), and $\Delta F_3^{(4)}$: $(\mathbf{q}_1,\mathbf{q}_2,-\mathbf{q}_1,-\mathbf{q}_2)$ (type D). Their combinatorial multiplicities are as follows:

V_1+V_2: four ways to place $\mathbf{q}_1$, two ways to place $-\mathbf{q}_1$ next to it, and two ways to place $\pm\mathbf{q}_2$, for a total of 16. Hence there are eight diagrams of each type.

D: four ways to place $\mathbf{q}_1$, two ways to place $\pm\mathbf{q}_2$. Total multiplicity is eight.

Therefore, the mutual interaction term is

$$\sum_{i<j}(8V_1+8V_2+8D)|\rho_{\mathbf{q}_i}|^2|\rho_{\mathbf{q}_j}|^2 \tag{B5}$$

$$=\sum_{i\neq j}(4V_1+4V_2+4D)|\rho_{\mathbf{q}_i}|^2|\rho_{\mathbf{q}_j}|^2. \tag{B6}$$

Notice that in the limit $\mathbf{q}_i\to\mathbf{q}_j$, $V_1\to B$, and $(V_2,D)\to A$. Hence, going back to the original notation in terms of $u(\alpha)$, we find that the full fourth-order GL term is

$$\delta F^{(4)}=\frac{1}{2}\sum_{i\neq j}u(\alpha_{ij})|\rho_{\mathbf{q}_i}|^2|\rho_{\mathbf{q}_j}|^2+\frac{1}{4}\sum_i u_0|\rho_{\mathbf{q}_i}|^2,$$

where $u(\alpha)=8(V_1+V_2+D)$ and $u_0=u(\alpha=0)$ (it can be shown explicitly that the limit $\alpha\to 0$ is continuous at finite temperature).

The interaction functions can be obtained by a mixture of analytical and numerical integration. The frequency summations could be performed with the help of contour integration,

$$\begin{aligned}\{V_1,V_2\}=\frac{v_{q_0}^4|\rho_{q_1}|^2|\rho_{q_2}|^2}{4}\sum_k&\frac{n_F(\epsilon_1)}{(\epsilon_1-\epsilon_2)^2(\epsilon_1-\epsilon_4)}\\&+\frac{n_F(\epsilon_4)}{(\epsilon_4-\epsilon_1)(\epsilon_4-\epsilon_2)^2}-\frac{n_F(\epsilon_2)}{(\epsilon_2-\epsilon_1)^2(\epsilon_2-\epsilon_4)}\\&-\frac{n_F(\epsilon_2)}{(\epsilon_2-\epsilon_1)(\epsilon_2-\epsilon_4)^2}\\&+-\frac{n_F'(\epsilon_2)}{(\epsilon_2-\epsilon_1)(\epsilon_2-\epsilon_4)},\end{aligned} \tag{B7}$$

and

$$\begin{aligned}D=\frac{v_{q_0}^4|\rho_{q_1}|^2|\rho_{q_2}|^2}{4}\sum_k&\frac{n_F(\epsilon_1)}{(\epsilon_1-\epsilon_2)(\epsilon_1-\epsilon_3)(\epsilon_1-\epsilon_4)}\\&+\frac{n_F(\epsilon_2)}{(\epsilon_2-\epsilon_1)(\epsilon_2-\epsilon_3)(\epsilon_2-\epsilon_4)}\\&+\frac{n_F(\epsilon_3)}{(\epsilon_3-\epsilon_1)(\epsilon_3-\epsilon_2)(\epsilon_3-\epsilon_4)}\\&+\frac{n_F(\epsilon_4)}{(\epsilon_4-\epsilon_1)(\epsilon_4-\epsilon_2)(\epsilon_4-\epsilon_3)}.\end{aligned} \tag{B8}$$

The numerical integration over momenta has to be done with care due to singular denominators. We found that numerical integration performs the best using the above forms of $\Delta F^{(4)}$ after introducing regularization $\frac{1}{(\epsilon_3-\epsilon_1)}\to \mathrm{Re}\frac{1}{(\epsilon_3-\epsilon_1+i\Gamma)}$, with $\Gamma=10^{-15}$ using the MATLAB 3D integration routine.

In 3D, there is a possibility of noncoplanar interaction diagrams. They arise only if there are nontrivial $\{\mathbf{q}_1,\ldots,\mathbf{q}_4\}$ that add up to 0. Such diagrams exist, for example, for fcc lattice, which has reciprocal bcc. There are eight bcc reciprocal vectors, which can be split into two distinct quadruplets (tetrahedra). Each has total $4!=24$ multiplicity. In the case of fcc, by symmetry, all diagrams have the same value and each has the same expression as D above. Let us name it $D_\square$. Then, in Eq. (4), $w=24D_\square$. The relative magnitude of coplanar and noncoplanar terms is obviously important. In Fig. 2, we plotted $u(\alpha)/8$ and, in Fig. 3, $w/24$.

APPENDIX C: VARIATIONAL CRYSTALLINE STATES

We have considered the following variational states (N is the number of $\pm\mathbf{q}_i$ pairs; see Fig. 5):

(i) Smectic or stripe: $N=1$.

(ii) Columnar: $N=2$. One neighbor at optimal angle $\alpha_{\min}$.

(iii) Rhombohedral: $N=3$. Two neighbors at optimal angle $\alpha_{\min}$.

(iv) bcc lattice (fcc reciprocal): $N=6$. Four neighbors with $\alpha=\pi/3$, one with $\alpha=\pi/2$.

(v) fcc lattice (bcc reciprocal): $N=4$. Three neighbors with $\alpha=\cos^{-1}(1/3)$.

(vi) iQC: $N=6$. Five neighbors with $\alpha_i\approx 63.4^\circ$.

(vii) Edge-icosahedral (momenta are the edges of icosahedron—favored by cubic interaction which we neglect): $N=15$. Four neighbors with $\alpha=60^\circ$, four neighbors with $\alpha=72^\circ$, four neighbors with $\alpha=36^\circ$, and two neighbors with $\alpha=90^\circ$. In the energy, there are noncoplanar terms present; we did not include this contribution since the energy of these

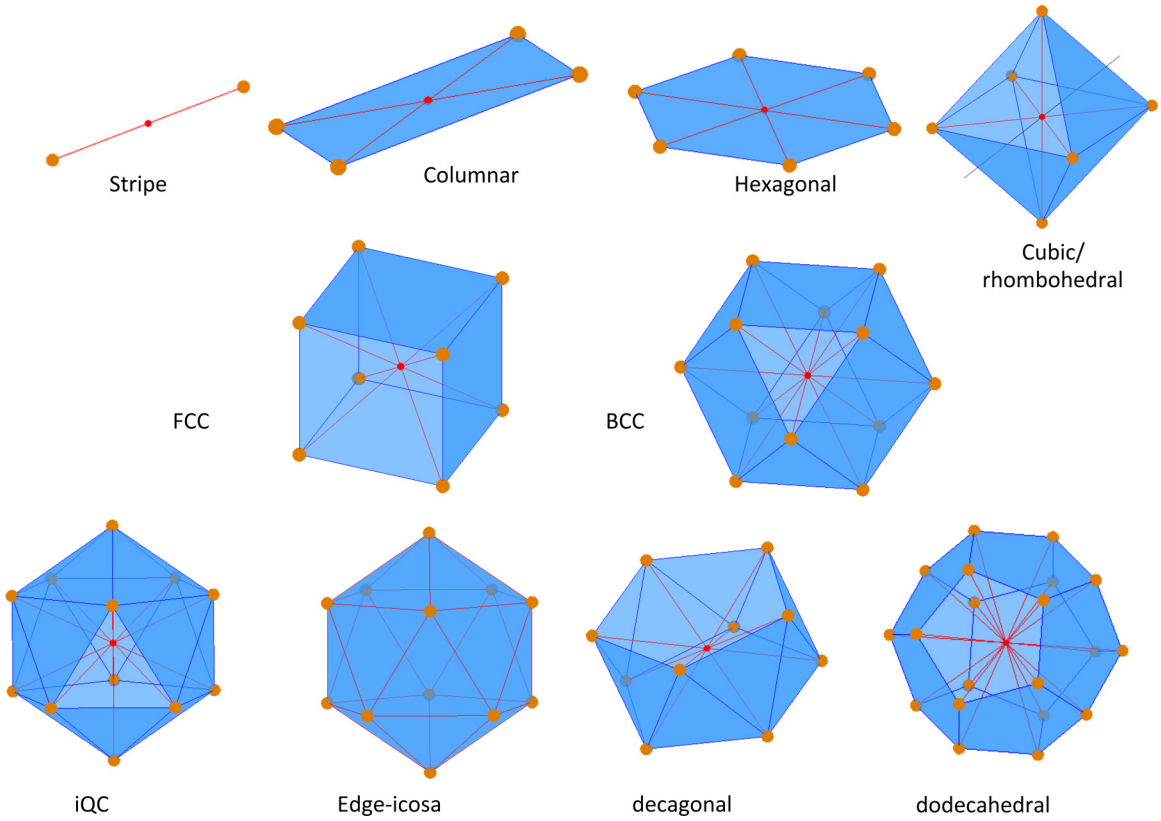

FIG. 5. Primary reciprocal lattice shells of variational states that we considered. Reciprocal vectors are indicated by red lines that start from the red sphere and end at golden spheres. Within the assumptions of weak crystallization theory, only such vectors, which all have equal length, contribute to crystallization energy. Clarifications: (1) vertices of perfect octahedron represent the primary reciprocal shell of a cubic state; general rhombohedral case can be obtained by linear dilatation or contraction along the axis connecting centers of opposite triangular faces (black line). (2) Reciprocal vectors of the edge-icosahedral state are, as the name implies, edges of icosahedron, shown in red.

states is relatively too high (due to many suboptimal angles α) and the noncoplanar contribution is weighted by small factor N^{-2}.

(viii) Decagonal (same as iQC, but with one vector pair missing): $N = 5$. Four neighbors at icosahedral angles α_i.

(ix) Dodecahedral in momentum space: $N = 10$. Three neighbors with $\alpha_1 \approx 41.8^\circ$, six neighbors with $\alpha_2 \approx 70.5^\circ$.

(x) Hexagonal: $N = 3$. Two neighbors at 60°.

APPENDIX D: SPLITTING PEAKS

Here we show that splitting of one Bragg peak into a pair is unfavorable. This is an immediate consequence of $u(\alpha)$ being smooth as $\alpha \to 0$, as is the case for electron-mediated and local interactions. Indeed, assume that there is an energetically favorable (possibly multi-$\mathbf{q}$) configuration with a spot at $\mathbf{q}_0$ with amplitude $\rho_{\mathbf{q}_0}$. Now, suppose we split it into two at $\mathbf{q}_0'$ and $\mathbf{q}_0''$, both approximately equal to $\mathbf{q}_0$. To keep the interaction with the other momentum components unchanged (we assumed it to be optimal), we need $|\rho_{\mathbf{q}_0'}|^2 + |\rho_{\mathbf{q}_0''}|^2 = |\rho_{\mathbf{q}_0}|^2$. That keeps the second order (r) and the interaction with distant q components intact. However, instead of the original self-interaction, we now have $u_0|\rho_{\mathbf{q}_0}|^4 \to u_0|\rho_{\mathbf{q}_0''}|^4 + 4u(\alpha)|\rho_{\mathbf{q}_0'}|^2|\rho_{\mathbf{q}_0''}|^2 \approx u_0(|\rho_{\mathbf{q}_0'}|^2 + |\rho_{\mathbf{q}_0''}|^2)^2 + 2u(\alpha)|\rho_{\mathbf{q}_0'}|^2|\rho_{\mathbf{q}_0''}|^2$. Hence, the energy goes up, and splitting is not favored for $u_0 > 0$. Indeed, the crystallization simulations starting from random initial conditions show the extinction behavior: large Bragg peak suppresses its smaller neighbors, leaving in the end only a small number of spots that correspond to a (q)crystal.

APPENDIX E: DISTORTED IQC STATE

To explore the stability of the iQC state with respect to distortions away from perfect icosahedron, let us expand the interaction energy in the vicinity of the iQC:

$$E_{\text{int}} = \sum_{i<j} u(\alpha_{ij})|\rho_i|^2|\rho_j|^2.$$

For the sake of argument, we will neglect the fact that the amplitudes of the order parameter can also react to distortions—this will only further lower the energy of the distorted state. Then, defining $\delta_{ij} = \alpha_{ij} - \alpha_0$,

$$E_{\text{int}} = E_0 + u'(\alpha_0)\sum_{i<j}\delta_{ij} + 0.5u''(\alpha_0)\sum_{i<j}\delta_{ij}^2 + \cdots.$$

Now we can choose convenient coordinates for the Bragg peaks on the sphere and explore whether the energy can be lowered by a distortion. Both the first and the second derivative terms define quadratic forms with non-negative eigenvalues (due to the nonlinear dependence of δ_{ij} on local coordinates, even the first-order term

produces quadratic form upon expansion). Out of 12 total eigenvalues, the quadratic form of $\sum_{i<j}\delta_{ij}$ has only four nonzeros; in contrast, $\sum_{i<j}\delta_{ij}^2$ has only three zero modes that correspond to rigid global rotations. When put together, for $u'(\alpha_0) < -(2/3)u''(\alpha_0)$, negative stiffness modes emerge, signifying distortive instability of icosahedron. The strongest instability occurs at the largest possible quasimomenta, $\pm 4\pi/5$. At the critical point $u'(\alpha_0) = -(2/3)u''(\alpha_0)$, four zero modes simultaneously appear, forming a flat zero-frequency band as a function of quasimomentum on icosahedron.

Hence, the conclusion is that even if $u(\alpha)$ reaches the minimum at a nonicosahedral angle, the iQC remains (at least) locally stable for $u' > 0$ ("tensile strain" between Bragg peaks), and even for "compressive strain" it remain stable until a critical value of negative u' is reached.

[1] F. A. Lindemann, Phys. Z **11**, 609 (1910).
[2] T. V. Ramakrishnan and M. Yussouff, Phys. Rev. B **19**, 2775 (1979).
[3] B. B. Laird, J. D. McCoy, and A. D. J. Haymet, J. Chem. Phys. **87** 5449 (1987).
[4] P. M. Chaikin and T. C. Lubensky, *Principles of Condensed Matter Physics*, Vol. 1 (Cambridge University Press, Cambridge, 2000).
[5] E. Kats, V. V. Lebedev, and A. Muratov, Phys. Rep. **228**, 1 (1993).
[6] P.-G. de Gennes, *Simple Views on Condensed Matter*, Vol. 8 (World Scientific, Singapore, 1998).
[7] S. Alexander and J. McTague, Phys. Rev. Lett. **41**, 702 (1978).
[8] W. Hume-Rothery, J. Inst. Met. **35**, 295 (1926).
[9] H. Jones, Proc. Phys. Soc. London **49**, 250 (1937).
[10] D. Shechtman, I. Blech, D. Gratias, and J. W. Cahn, Phys. Rev. Lett. **53**, 1951 (1984).
[11] D. Levine and P. J. Steinhardt, Phys. Rev. Lett. **53**, 2477 (1984).
[12] D. DiVincenzo and P. Steinhardt, *Quasicrystals: The State of the Art* (World Scientific, Singapore, 1999).
[13] C. Janot, *Quasicrystals* (Springer, New York, 1994).
[14] H.-R. Trebin, *Quasicrystals: Structure and Physical Properties* (Wiley, New York, 2006).
[15] G. T. De Laissardière, D. Nguyen-Manh, and D. Mayou, Prog. Mater. Sci. **50**, 679 (2005).
[16] A. P. Tsai, Sci. Technol. Adv. Mater. **9**, 013008 (2008).
[17] U. Mizutani, Y. Sakabe, T. Shibuya, K. Kishi, K. Kimura, and S. Takeuchi, J. Phys. Condens. Matter **2**, 6169 (1990).
[18] A. P. Smith and N. W. Ashcroft, Phys. Rev. Lett. **59**, 1365 (1987).
[19] J. Friedel, Helv. Phys. Acta **61**, 538 (1988).
[20] P. Bak, Phys. Rev. Lett. **54**, 1517 (1985).
[21] P. A. Kalugin, A. Y. Kitaev, and L. S. Levitov, JETP Lett. **41**, 145 (1985).
[22] M. V. Jarić, Phys. Rev. Lett. **55**, 607 (1985).
[23] N. D. Mermin and S. M. Troian, Phys. Rev. Lett. **54**, 1524 (1985).
[24] S. Narasimhan and T.-L. Ho, Phys. Rev. B **37**, 800 (1988).
[25] S. Sachdev and D. R. Nelson, Phys. Rev. B **32**, 4592 (1985).
[26] For analysis of the local weak crystallization model with the condition relaxed, see [24] .
[27] L. P. Gorkov, Sov. Phys. JETP **9**, 1364 (1959).
[28] P. Chen and J. Vinals, Phys. Rev. E **60**, 559 (1999).
[29] A. C. Skeldon and G. Guidoboni, SIAM J. Appl. Math. **67**, 1064 (2007).
[30] S. A. Brazovskii, Sov. Phys. JETP **41**, 85 (1975).
[31] P. Hohenberg and W. Kohn, Phys. Rev. **136**, B864 (1964).
[32] J. Hafner, Phys. Rev. B **21**, 406 (1980).
[33] L. Shulenburger, M. P. Desjarlais, and T. R. Mattsson, Phys. Rev. B **90**, 140104 (2014).
[34] Y. Singh, Phys. Rep. **207**, 351 (1991).
[35] U. Mizutani, T. Takeuchi, and H. Sato, Prog. Mater. Sci. **49**, 227 (2004).
[36] M. A. Ruderman and C. Kittel, Phys. Rev. **96**, 99 (1954).
[37] T. Kasuya, Prog. Theor. Phys. **16**, 45 (1956).
[38] K. Yosida, Phys. Rev. **106**, 893 (1957).